Dalton Transactions

ROYAL SOCIETY OF CHEMISTRY

PAPER

View Article Online
View Journal | View Issue

Cite this: *Dalton Trans.*, 2025, **54**, 14587

Investigating the DNA binding properties of two new Ru^{II}(dppz) complexes incorporating the facially coordinated ligands tris(pyridin-2-yl) methylamine and di(pyridin-2-yl)methylamine

Thomas S. Andrews, Craig Robertson, Anthony J. H. M. Meijer * and Jim A. Thomas *

By employing the facially coordinated tris(pyridin-2-yl)methylamine ligand, a route to the synthesis of the complex ([Ru(tpyma)(dppz)(py)]$^{2+}$ (dppz = dipyrido[3,2-*a*:2′,3′-*c*]phenazine) py = pyridine) is reported. Detailed NMR spectroscopy and crystallographic studies reveal that tpyma coordinates to the metal ion through a tridentate (2py, NH_2), not (3py), binding motif. Subsequently, the synthesis of an analogous complex containing di(pyridin-2-yl)methylamine, dipyma, confirmed that it too is a (2py, NH_2) tripodal ligand. In non-aqueous solvents both complexes display emission from the Ru^{II} → (dppz)-based ^{3}MLCT excited state. Computational studies reveal that the metal centre of the dipyma complex is more polar than its tpyma analogue and also provide insights into why tpyma does not coordinate to the Ru^{II}(dppz) through a (3py) motif. In aqueous solutions the complexes bind to duplex DNA through intercalation with affinities that are entirely comparable to [Ru(bpy)$_2$(dppz)]$^{2+}$. However, while the tpyma complex displays a DNA light switch effect, the DNA-induced increase in emission from the dipyma complex is significantly lower. This effect is attributed to the different electronic and steric properties of tpyma and dipyma.

Received 16th May 2025,
Accepted 6th September 2025

DOI: 10.1039/d5dt01159k

rsc.li/dalton

Introduction

After the first report on the original "DNA light switch" [Ru(bpy)$_2$(dppz)]$^{2+}$ (bpy = 2,2′-bipyridine, dppz = dipyrido[3,2-*a*:2′,3′-*c*]phenazine),[1] complexes containing the Ru^{II}(dppz) moiety have attracted considerable research attention.[2–4] Thanks to the combination of the DNA intercalating properties of the extended dppz ligand and a solvent-sensitive Ru → dppz-based ^{3}MLCT excited state, the complex is non-emissive in aqueous solution until it binds to DNA when its luminescence is "switched on".[5–13] Consequently, similar effects have been observed for other d^6-metal complexes; for example, systems containing Re^{I}(dppz) and Ir^{III}(dppz) fragments, and numerous complexes containing ligands related to dppz.[14–18] Over recent years, oligonuclear derivatives have also been studied and they often display enhanced DNA binding affinities.[19–23] This work has produced novel live-cell probes, as well as chemotherapeutic and phototherapeutic leads.[24–30]

In a contribution to these studies, the Thomas group has been using achiral complexes as "building blocks" to develop facile routes in the construction of oligonuclear complexes containing Ru^{II}(dppz) and related fragments. Using this approach, complexes such as [RuCl(tpm)(dppz)]$^+$,[31] [RuCl(tpm)(dppn)]$^+$,[32,33] and [ReCl(CO)$_3$(dppz)], (tpm = tris(pyrazolyl)methane), (dppn = benzo[i]dipyrido[3,2-*a*:2′,3′-*c*]phenazine) were used as synthons to yield linked homo[34–37] and heteronuclear[38–40] systems.

With the goal of identifying new building blocks with modulated chemical, photophysical and biophysical properties in mind, studies aimed at synthesizing related mononuclear tpyma complexes (tpyma = tris(pyridin-2-yl)methylamine)[41] that could potentially function as new Ru^{II}(dppz) synthons in the construction of oligomeric multifunctional DNA-binding systems are described herein.

This ligand was chosen for several reasons. First, the use of tridentate ligands can remove the complications due to the chirality of [Ru(bpy)$_3$]$^{2+}$ type building blocks. Secondly, as tpyma contains three linked pyridyl-based donor groups, it should strongly chelate to Ru^{II} centres but, unlike the much-employed terpyridine (tpy), it is linked through a central carbon bridgehead, giving the ligand more flexibility. This potentially alleviates issues around ligand strain and chelate bite angles that cause the excited states of Ru(tpy) based systems to display negligible luminescence.[42] Thirdly and finally, this ligand possesses a functionalized bridgehead that

Chemistry, School of Mathematics and Physical Science, University of Sheffield, Brook Hill, Sheffield, S3 7HF, UK. E-mail: a.meijer@sheffield.ac.uk, james.thomas@sheffield.ac.uk

could be used for further derivatization of the free ligands or coordinated complexes.

A number of related tripodal ligands, such as tris(pyridin-2-yl)methane and tris(pyridin-2-yl)amine have been widely studied and are known to coordinate to ruthenium;[43] yet, surprisingly few studies involving tpyma have been reported since its first synthesis in 1998.[41] After the original report, its coordination chemistry with Cu(I), Cu(II) and Zn(II) centres was explored, where it was found to display three different coordination modes: bidentate (py, NH_2), tridentate (2py, NH_2), and tridentate (3py).[44]

More recently tpyma formed the recognition motif for an electrode based Ti^{III} sensor, where it displays tridentate (3py) binding.[45] However, despite the huge number of studies on other polypyridyl ligands, until now no studies involving d^6 metal ions with tpyma have been reported.

In this report, the route to the synthesis of a complex containing this ligand is reported. In these studies, it was found that although the ligand coordinates to Ru in a facial manner, it does so through the tridentate (2py, NH_2) binding mode. This observation prompted an investigation into the synthesis of a complex containing di-2-pyridylmethanamine, dipyma, as a tripodal ligand. The structural, photophysical, and DNA-binding properties of both complexes were then investigated, which revealed that they display differing DNA binding responses which can be explained by a consideration of the electronic and steric effects of coordinated tpyma and dipyma.

Results and discussion

Synthesis and characterization

We previously synthesized $[RuCl(tpm)(NN)]^+$ (where NN = bidentate polypyridyl ligands) using $[RuCl_3(tpm)]$ as a starting material.[31] However, although the direct reaction of $RuCl_3$ and tpm is convenient,[46] the yield of the complex using this route is only moderate. Therefore, one aim of this study was to investigate alternative routes toward the synthesis of analogous $[RuCl(tpyma)(NN)]^+$ complexes. We found an adaption of methods reported by the Keyes group using $[RuCl_2(DMSO)_4]$ as a starting material provided a reliable route toward these targets.[47] In this route a bidentate ligand such as bpy, phen, or dppz was first reacted with $[RuCl_2(DMSO)_4]$ to yield the neutral complex $[RuCl_2(NN)(DMSO)_2]$ in essentially quantitive yield (>95%). Subsequent reaction of this product with tpyma in ethylene glycol for one hour yielded $[RuCl(tpyma)(NN)]^+$.

Although yields in this second step were lower (~45–50%), yields over the two steps were still higher than the direct route and more convenient in terms of work up. This complex could then be reacted with a suitable monodentate ligand, such as pyridine to yield $[Ru(tpyma)(NN)(py)]^{2+}$ – Scheme 1.

The coordination mode of tpyma in these new complexes was first determined through NMR studies, which are best illustrated through a consideration of the 2D COSY ^{1}H-NMR spectrum of $[Ru(tpyma)(dppz)(py)](PF_6)_2$ – Fig. 1 – which was also used to absolutely assign the entire structure.

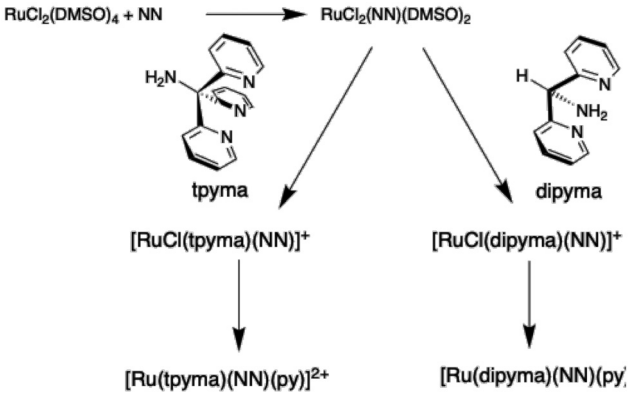

Scheme 1 Synthetic route employed in the syntheses of new Ru^{II} tpyma and dipyma complexes reported in this study. NN = bpy, phen, or dppz and py = pyridine.

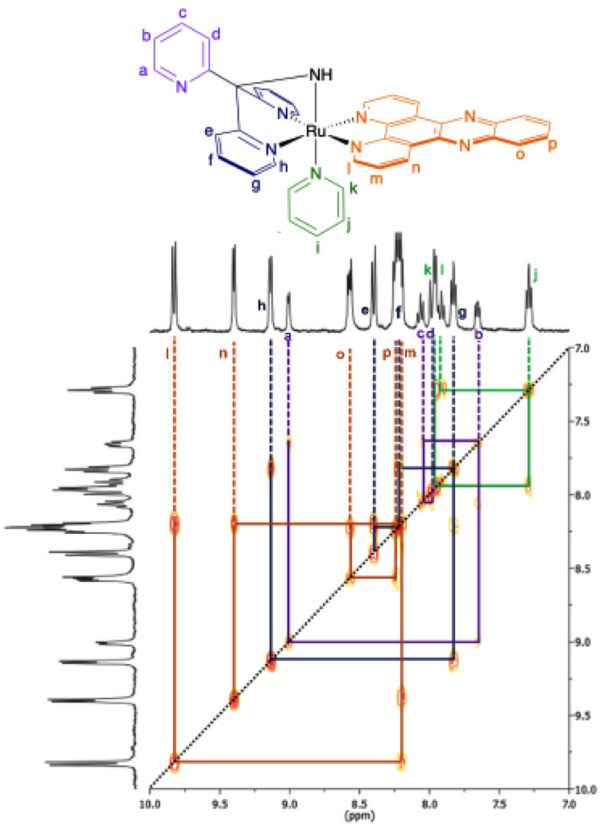

Fig. 1 400 MHz COSY ^{1}H NMR of $[Ru(tpyma)(dppz)(py)](PF6)_2$ in d^6-acetone with coupled protons connected by lines.

The NMR spectrum clearly reveals that not all the pyridyl rings are coordinated to the Ru^{II} centre. Most strikingly, protons **a–d** are clearly the only ring system in the molecule to consist entirely of single proton environments, as the ring is bisected by the plane of symmetry on the molecule. These protons can be distinguished from each other through their splitting patterns, coupling constants, and also their proximity

to the nitrogen atom: as the closest proton to nitrogen **a** will be most deshielded it can be assigned to the peak at highest ppm shift. The primary coupling to proton **b** forms a doublet, though some smaller coupling interaction with other protons can be seen.

The only other proton in the ring system that has one neighbour, thus forming a doublet, is proton **d**. As **d** shares a coupling value of 8.1 Hz with the triplet at 8.0–8.1 ppm this latter signal is assigned to proton **c**. The remaining proton **b** is assigned through a coupling constant of 4.8 Hz shared with proton **a**.

The protons of the coordinated ring systems, **e–h**, are assigned in a very similar way to **a–d** as, although they are shifted, they exhibit the same splitting and coupling patterns. Protons **e** and **h** are assigned to the doublet peaks at 9.2 ppm and 8.3 ppm shift, with proton **h** assigned to the more deshielded peak owing to its proximity to the nitrogen atom. The **h** doublet exhibits a coupling constant of 5.2 Hz, shared with the pseudo triplet peak at 7.7 ppm shift, thus this is assigned to its neighbour proton **g**. The remaining peak in the system shares a coupling value of 8.0 Hz with **e** confirming that it is due to proton **f**.

The other ring system that sits in the plane of symmetry is the monodentate pyridine ligand. Its protons, **i–k**, are distinguished as the only ring system that exhibits three proton environments, whereas all others have four. It also is the only system to integrate in a 2 : 2 : 1 pattern. These protons can be easily assigned their integral values and splitting patterns. Proton **i** is assigned to the only peak in the ring system with an integral value of one, as the other protons on the ring have an equivalent partner opposite, resulting in an integral value of two. Proton **k** is assigned to the doublet peak of the three in the ring system as it only has one neighbour. This leaves proton **j** as the pseudo triplet as it couples to both **i** and **k**.

Again, through a combination of cross-correlation, integrals, splitting pattens and coupling constants, dppz protons **l**, **m**, and **n** are easily identified in the COSY spectrum, with **l** being the down-field shifted signal due to its proximity to the metal coordinated N-donor. Similarly, protons **o** and **p**, are assigned through their proximity to the uncoordinated nitrogen atoms of dppz, with **o** being the most deshielded. They also exhibit a distinctive splitting pattern that is related to the magnetic non-equivalence of the protons. This is clearly observed for the peak relating to **o** but not for **p** which is part of a mixed signal.

Given the observation that tpyma coordinates to the Ru^{II} centre through a facial (2py, NH_2) binding mode, we investigated whether dipyma could be used as a facially coordinated ligand for this class of complexes. Again, reports on the coordination chemistry of this ligand are very sparse. The only previous study[48] involving ruthenium described the synthesis and electrochemical properties of the *meso* and *rac* isomers of $[Ru(dipyma)_2]^{2+}$ which showed that, in this case, it coordinates in a tridentate mode. The ligand was synthesized through the reported method[48] and the complexes $[RuCl(dipyma)(dppz)]^{+}$ and $[Ru(dipyma)(dppz)(py)]^{2+}$ were obtained through the same methods used to synthesized their tpyma analogues. Again, NMR studies confirmed that dipyma also coordinates to Ru^{II} through a facial (2py, NH_2) binding mode – see SI for spectra.

X-ray crystallography

The binding modes of both tpyma and dipyma were confirmed through crystallographic studies on the hexafluorophosphate salts of $[Ru(tpyma)(dppz)(py)]^{2+}$ and $[Ru(dipyma)(dppz)(py)]^{2+}$.

Crystals of $[Ru(tpyma)(dppz)(py)](PF_6)_2$ were obtained from vapor diffusion at 3 °C using nitromethane as the solvent and diethyl ether as the anti-solvent. The large unit cell contains eight cations with dppz ligands and counterions. The complex cations display off-set stacking on top of each other through the extended dppz ligand – see Fig. 2.

In terms of the cation structure, coordination of tpyma produces a significant distortion away from ideal octahedral geometry. The N–Ru–N bond angles within the ligand are more acute than the ideal octahedral 90°; between the two pyridines this angle is 83.93(10)°, while the angles involving py-NH_2 are 77.17(10)° and 78.61(10)° respectively. The trans angle from NH_2 to the pyridine ligand (170.63(9)°) also reflects this distor-

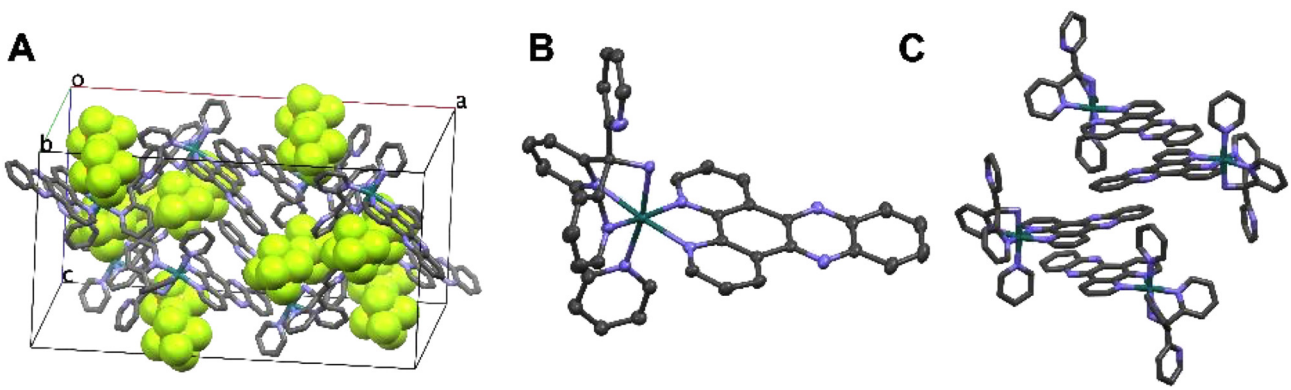

Fig. 2 X-ray crystal structure of $[Ru(tpyma)(dppz)(py)](PF_6)_2$. (A) The unit cell. (B) Thermal ellipsoid depiction of a cation in the structure. (C) Off-set stacking of cations involving dppz ligands. In all cases, hydrogen atoms removed to aid visualization.

tion. Each Ru–N bond lengths involving the tridentate ligand are similar, ranging from 2.057(3) Å to 2.093(2) Å.

The key feature of the $[Ru(tpyma)(dppz)(py)](PF_6)_2$ crystal structure is the aforementioned stacking that runs through the crystal: each complex is sits atop another through, slightly rotated, offset π–π interactions involving dppz ligands. The rotation in each step also avoids steric clashes between dppz and tpyma ligands of neighbouring cations.

Using the same vapor diffusion method used for this tpyma analogue, crystals of $[Ru(dipyma)(dppz)(py)]^{2+}$ were obtained – Fig. 3. Although the quality of the data set collected is too poor to provide any detailed analysis of bond length and angles (R = 17.7%), it confirms the connectivity in this complex is not bidentate, but the same as that in the tpyma complex, with dipyma acting as a tridentate (2py, NH_2) facial ligand. Again, the long-range order of the structure is dominated by stacking interactions between dppz moieties.

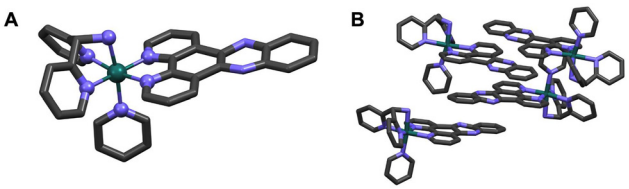

Fig. 3 X-ray crystal structure of $[Ru(dipyma)(dppz)(py)](PF_6)_2$. (A) Cation within the structure (B) stacking motif involving dppz ligands of these cations. Anions and hydrogen atoms removed to aid visualization.

Table 1 Optical properties of the two newly reported complexes

Complex[a]	Absorption (ε/M^{-1} cm^{-1}/10^3)	Assignment
$[Ru(tpyma)(dppz)(py)]^{2+}$	249 (sh)	π–π*
	276 (55.6)	π–π*
	318 (17.8)	π–π*
	352 (18.0)	π–π*
	361 (19.0)	π–π*
	370 (19.8)	π–π*
	426 (10.5)	MLCT
	472 (sh)	MLCT
$[Ru(dipyma)(dppz)(py)]^{2+}$	248 (sh)	π–π*
	275 (44.3)	π–π*
	318 (sh)	π–π*
	359 (15.2)	π–π*
	373 (16.1)	π–π*
	431 (8.2)	MLCT
	470 (sh)	MLCT

[a] Recorded at room temperature as hexafluorophosphate salts in acetonitrile.

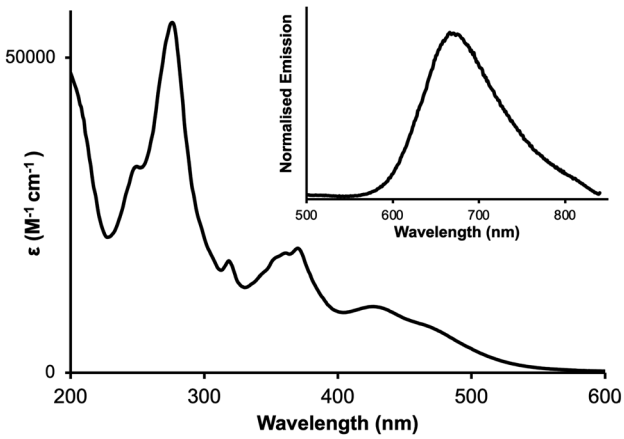

Fig. 4 UV-Vis spectrum of $[Ru(tpyma)(dppz)(py)](PF_6)_2$ in room temperature acetonitrile solution inset: emission spectrum in the same conditions on excitation at 426 nm.

Optical properties

The steady-state absorption and emission spectra of $[Ru(tpyma)(dppz)(py)]^{2+}$ and $[Ru(dipyma)(dppz)(py)]^{2+}$, recorded as their hexafluorophosphate salt in acetonitrile, are very similar – see Table 1.

Fig. 4 shows the relevant spectra for the tpyma complex; the absorption spectrum displays several intense peaks below 350 nm which are associated with π–π* transitions. A double humped band between 350–380 nm is characteristic of the dppz ligand. At longer wavelengths, a band centred at 426 nm with a shoulder at 472 nm, is observed. This is assigned to a Ru^{II} → (dppz)-based ^{1}MLCT excitation.

Photoexcitation into this ^{1}MLCT in acetonitrile solution results in a broad unstructured luminescence, centred at 670 nm for $[Ru(tpyma)(dppz)(py)]^{2+}$ and 668 nm for $[Ru(dipyma)(dppz)(py)]^{2+}$, which can be assigned to emission from the Ru^{II} → (dppz)-based ^{3}MLCT excited state. Notably, this is a red-shifted by ~60 nm compared to the parent $[Ru(bpy)_2(dppz)]^{2+}$.[1,49]

Computational studies

Prompted by the experimental structural studies, a series of DFT calculations on both structures using Gaussian 16 were carried out[50] and compared to the unobserved (3py) isomer of $[Ru(tpyma)(dppz)(py)]^{2+}$. The results for the experimentally observed structures are given in Fig. 5.

In these calculations the B3LYP-D3(BJ) functional,[51,52] was used with a combined basis set, consisting of an Stuttgart-Dresden ECP on Ru[53,54] and 6-311G(d,p)[55,56] on all other atoms, as used in previous work.[38,57] Bulk solvent was described with the IEFPCM method[58,59] using the parameters for MeCN, as implemented in Gaussian; see section S3 in the SI for full details.

As shown by Fig. 5(a) and (b) there is very little difference between the calculated and reported structures of the two complexes studied in this paper. These results also clearly show that the pendant uncoordinated py group does not really interact with the rest of the tpyma moiety. However, its presence does lead to differences in charge distribution within the complex; in particular, the partially positively charged hydrogen atoms on the amine moiety are not as available in $[Ru(tpyma)(dppz)(py)]^{2+}$ compared to $[Ru(dipyma)(dppz)(py)]^{2+}$. As discussed later, this

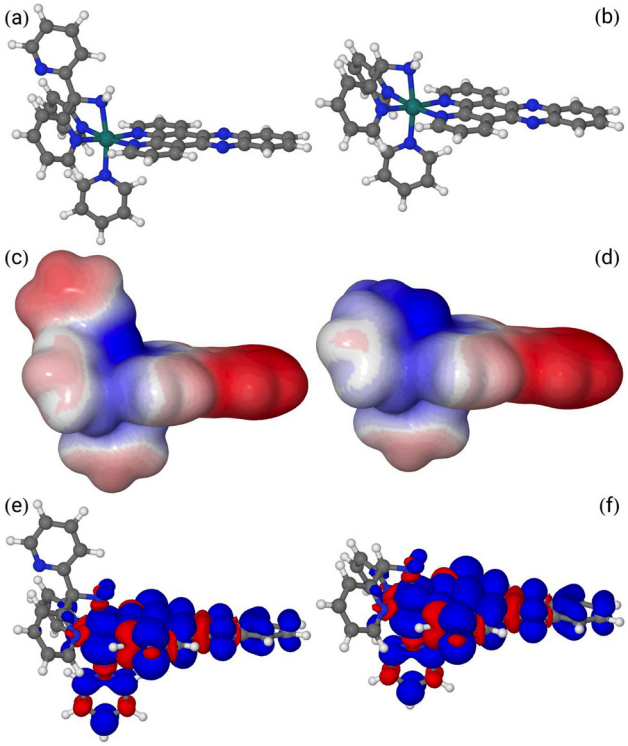

Fig. 5 Comparison between $[Ru(tpyma)(dppz)(py)]^{2+}$ (2py, NH_2) binding motif (left-hand column) and $[Ru(dipyma)(dppz)(py)]^{2+}$ (right-hand column). Panels (a) & (b): Calculated structures. Panels (c) & (d): Electrostatic potential mapped onto the 0.0004 electron density surface [max value: 0.25 (blue); min value 0.1 (red)]. Panels (e) & (f): Spin-density for the T_1 state.

observation may have implications for how this complex interacts with its surroundings and solvent molecules.

The T_1 spin density for both complexes is given in Fig. 5(e) and (f), showing that T_1 is an MLCT state relative to S_0. Again, there is very little difference between them, which is unsurprising, given the similar emission wave lengths discussed above. If the emission energy is approximated by the difference between the ground vibrational state energies for both complexes, these calculations give emission wave lengths of 637 and 635 nm, respectively which are in broad agreement with experiment and confirm that the electronic properties of the two complexes are very similar.

As noted above, $[Ru(tpyma)(dppz)(py)]^{2+}$ also has a potential isomer with a (3py) binding motif, which was investigated computationally. Its structure and electrostatic potential, mapped onto the electron density are given in Fig. 6. Although the structure features for the (3py) binding motif are as expected, surprisingly this binding motif is calculated to be 25.8 kJ mol^{-1} lower in energy (free energy difference: 20.1 kJ mol^{-1}) than the (2py, NH_2) experimentally-observed binding motif, suggesting that this isomer should dominate in solution.

Furthermore, extensive searching of other (2py, NH_2) binding motifs did not lead to any isomers which were more

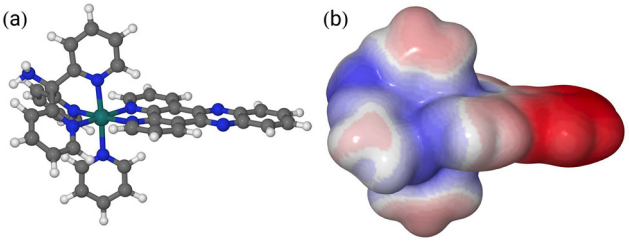

Fig. 6 (a) Calculated structure for $[Ru(tpyma)(dppz)(py)]^{2+}$ (3py) binding motif (b) electrostatic potential mapped onto the 0.0004 electron density surface [max value: 0.25 (blue); min value 0.1 (red)].

than 0.7 kJ mol^{-1} lower in energy than the isomer discussed above. A potential solution to this unexpected outcome lies in the mapped electrostatic potential shown in Fig. 6(b), which is significantly different from that shown in Fig. 5(c).

In particular, the hydrogen atoms of the pendant NH_2 group in the (3py) binding motif display lower Lewis base character and so are less available for hydrogen bonding compared to the (2py, NH_2) binding motif, suggesting the (3py) binding isomer would display attenuated interactions with solvents.

To test this hypothesis, a series of calculations were performed with one to four MeCN molecules forming part of an explicit solvation shell around the transition metal complexes. The results for a partial solvation shell of four MeCN molecules are shown in Fig. 7 for both binding motifs. We also explored 2 different orientations for the pendant py group in the (2py, NH_2) binding motif, but they were all significantly higher in energy – all the results are summarized in the SI – see sections S15 and S16 in the SI. Our calculations show that the MeCN molecules coordinating to $[Ru(tpyma)(dppz)(py)]^{2+}$ take up positions, which enhance van der Waals interactions to either the NH_2 hydrogen atoms or to the dppz π-system. We disregarded any potential binding in the dppz plane to its Lewis-basic nitrogens as interactions involving the two different possible binding motifs are expected to largely cancel out.

These calculations show that by binding to 4 MeCN molecules there is a 32.7 kJ mol^{-1} change in the relative stability of the two isomers so that the (2py, NH_2) binding motif is now 6.9 kJ mol^{-1} lower in energy than the 3py binding form.

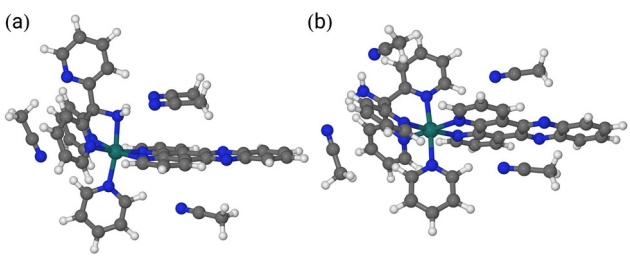

Fig. 7 Comparison of partial solvation shells around the two binding motifs for $[Ru(tpyma)(dppz)(py)]^{2+}$. Panel (a): (2py, NH_2) binding motif, relative energy: 0.0 kJ mol^{-1}. Panel (b): (3py) binding motif, relative energy: +6.9 kJ mol^{-1}.

However, most interestingly, our calculations show the importance that solvent plays in determining the relative stability of complexes, suggesting that solvent used in the synthesis of this class of complexes may influence the final complex obtained – an issue that will be explored in a future study.

DNA binding studies

Absorption and emission titrations of the chloride salts of both complexes with calf-thymus DNA (CT-DNA) in an aqueous tris buffer were then carried out.

Addition of CT-DNA produced similar distinctive changes in the absorption bands of both complexes. An example of the changes observed for $[Ru(tpyma)(dppz)(py)]^{2+}$ in these titrations is shown in Fig. 8 – see SI for the analogous titration with for $[Ru(dipyma)(dppz)(py)]^{2+}$ (Fig S2.1).

By fitting these changes to the much-used McGhee–Von Hippel model, MVHM, for noncooperative binding to a non-isotropic lattice,[60] estimates of binding affinity, K_b, and site size in base-pairs, S, were obtained. Such an analysis for $[Ru(tpyma)(dppz)(py)]^{2+}$ led to $K_b = 1.66 \times 10^6$ M^{-1} and $S = 1.1$ bp; whilst a similar analysis of the data for $[Ru(dipyma)(dppz)(py)]^{2+}$ led to $K_b = 0.7 \times 10^6$ M^{-1} and $S = 1.1$ bp.

The large hypochromicity changes observed in the MLCT (~20%) and dppz-associated (27%) bands, accompanied by an 8 nm red-shift in the MLCT peak are typical for Ru^{II}(dppz) units on intercalation into DNA. Although their estimated binding site sizes are lower than expected for conventional intercalators – in which site-exclusion effects are expected to restrict any binding site to a minimum of 3 bp – thanks to external stacking interactions lower site sizes, even below one bp, have been reported for many DNA intercalating metal complexes.

To confirm that the complexes are intercalators relative viscometry experiments were carried out. Shorter sequence of CT-DNA, prepared by ultrasound treatment, act as a rod-like polymer and thus any change in the viscosity of their aqueous solutions can be related to the average contour length of the dissolved duplex. Unlike groove binders, intercalators increase duplex contour length, therefore provoking an increase in relative specific viscosity.[61–63] Hence the addition of the complexes on linearized CT-DNA was compared to the changes produced by the well-known groove binder Hoechst 33258 and the intercalator ethidium bromide.

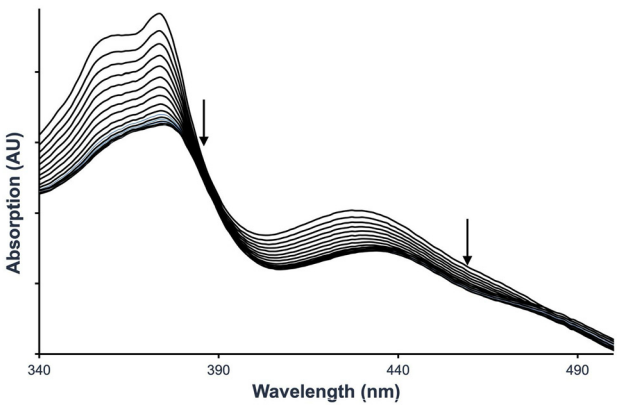

Fig. 8 Changes in the MLCT region of the absorption spectrum of $[Ru(tpyma)(dppz)(py)]Cl_2$ on progressive addition of CT-DNA at room temperature. Conditions: 1.54 μM solution of complex in tris buffer (5 mM tris and 25 mM NaCl at pH 7.5).

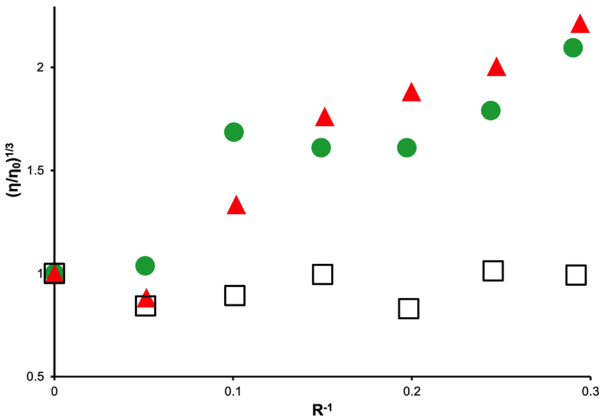

Fig. 9 Plot of relative viscosity $(\eta/\eta_0)^{1/3}$ of linearized CT-DNA *versus* 1/*R* at 25 °C. Changes induced on addition of ethidium bromide (●), Hoechst 33258 (□), or $[Ru(tpyma)(dppz)(py)]^{2+}$ (▲).

As the data for $[Ru(tpyma)(dppz)(py)]^{2+}$ illustrates, Fig. 9, progressive addition of the complex induces relative viscosity changes that are almost identical to those produced by ethidium bromide, confirming that – as expected – these complexes are intercalators. This prompted us to look at how DNA binding affected the luminescence of the complexes; interestingly, it was found that although the two complexes show similar DNA-induced absorption changes, their luminescence responses are distinctly different.

As expected for this class of metallo-intercalator, complex $[Ru(tpyma)(dppz)(py)]^{2+}$ exhibits a classic DNA light-switch effect; the complex is non-luminescent in water but progressive addition of CT-DNA results in increasingly intense ^{3}MLCT emission – Fig. 10A. At saturation, the luminescence is centred at 660 nm, which represents a red shift of >40 nm compared to $[Ru(bpy)_2(dppz)]^{2+}$ but is very similar to $[Ru(tpm)(dppz)(py)]^{2+}$ in similar conditions.[31] Fits of this data to MVHM led to binding parameter estimates of $K_b = 1.73 \times 10^6$ M^{-1} and $S = 1.94$. Within experimental error, the estimated K_b obtained in this fit is in good agreement with the absorption titration value.

On the other hand, the site size obtained from the luminescent titration is larger and closer to that expected for a classical intercalator, indicating that – as might be expected – any external binding mode has less effect on the intercalation-induced changes in emission of the complex.

Contrastingly, as shown in Fig. 10B, there is little change in the emission of $[Ru(dipyma)(dppz)(py)]^{2+}$, even on addition of excess CT-DNA, although it is important to note that the emission is not quenched by binding. So, although a titration can be performed, the emission spectra for the dipyma complex

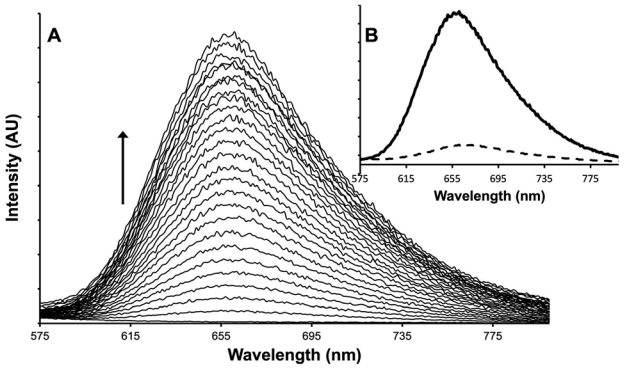

Fig. 10 A. Changes in emission of a 1.52 μM solution of [Ru(tpyma)(dppz)(py)]$^{2+}$ on progressive addition of CT-DNA B. Comparison of the emission from solutions of the same concentration of [Ru(tpyma)(dppz)(py)]Cl_2 (bold line) and [Ru(dipyma)(dppz)(py)]Cl_2 (dashed line) on addition of excess CT-DNA. Conditions: tris buffer (5 mM tris and 25 mM NaCl at pH 7.5) at room temperature.

are very noisy (see Fig S2.2), likely due to the observed emission is close to instrumental detection limits. The differing emission response of the two complexes to DNA binding is striking, particularly as the emission of their hexafluorophosphate salts in MeCN at very similar. There are several possible explanations for this observation.

The emission of metal complexes with high-energy excited states that interact with DNA can be quenched by redox processes involving guanine sites;[64–67] however, this possibility can be discounted as the complex does show some increase in its emission on addition of DNA. A second possible explanation involves a consideration of the excited states of [Ru(dipyma)(dppz)(py)]$^{2+}$.

A range of experimental and theoretical reports on [Ru(bpy)$_2$(dppz)]$^{2+}$ and its derivatives have indicated that the light-switch effect is due to an interplay between two close lying excited states: the "bright" and "dark" states.[5,6,8,68] Although all these studies agree that the bright state can be assigned to a MLCT and that the dark state is localized over the dppz ligand, the nature of the dark state is still debated; the two main possibilities being a second MLCT or a ππ* state.

Such studies have demonstrated that for light-switching to occur the dark state must lie close to the bright state so that it can be thermally accessed. If the dark state is significantly lower in energy than the bright state, then light-switching is not observed. To investigate this further, we performed a series of time-dependent DFT calculations.

In these computational studies, we took two different approaches. The first focussed solely on the complexes whereas in the second approach the complexes were intercalated into a simple G–C/C–G DNA step. Due its significantly lowered computational costs, in these latter calculations the optimized structures were obtained using GFN2-xTB [69] – see SI for computational details.

In both approaches the first three triplet states from the S_0 geometry were solved for, with the assumption that geometric relaxation is slow enough that the S_0 geometry will be representative of that involved in emission. An analysis of the GFN2-xTB calculations for intercalated [Ru(dipyma)(dppz)(py)]$^{2+}$ and [Ru(tpyma)(dppz)(py)]$^{2+}$, confirmed that the S_0 and T_1 geometries are very similar (Tanimoto shape coefficients larger than 0.97). Overlays for these structures are given in Fig. 11.

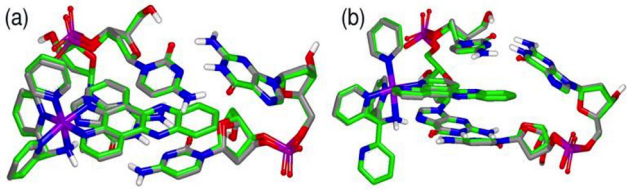

Fig. 11 Overlay generated with vROCS[70] between the S_0 geometries (grey) and the T_1 geometries (colour) for intercalated [Ru(dipyma)(dppz)(py)]$^{2+}$ (panel a) and [Ru(tpyma)(dppz)(py)]$^{2+}$ (panel b). For both panels the Tanimoto shape coefficient is larger than 0.97. In both cases the lower base pair is G–C, whereas the upper base pair is C–G.

The transition densities for the calculated transitions are shown in Fig. 12 (for the free complexes in acetonitrile) and Fig. 13 (for the intercalated complexes in water).

As is clear from Fig. 12, the character of the T_1–T_3 states relative to the S_0 state is similar for both free complexes with the transitions into these states from the S_0 state MLCT in nature. This is consistent with the spin densities for the T_1 state given in Fig. 5(e) and (f). A comparison of Fig. 12 and 13 reveals that intercalation into the G–C/C–G DNA step has a

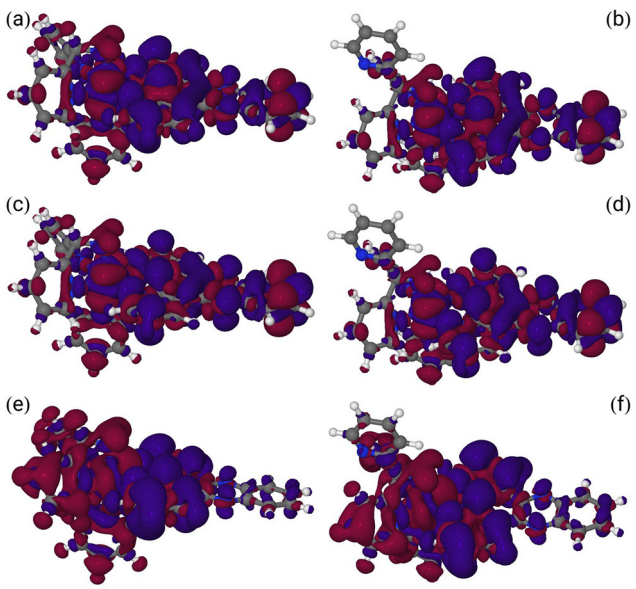

Fig. 12 Transition densities from the S_0 state in the S_0 geometry for [Ru(dipyma)(dppz)(py)]$^{2+}$ (left hand column) and [Ru(tpyma)(dppz)(py)]$^{2+}$ (right hand column) in acetonitrile. Panels (a) & (b): S_0 to T_1. Panels (c) & (d): S_0 to T_2. Panels (e) & (f): S_0 to T_3. In all cases, an singlet closed shell reference wave function was used. Red indicates density loss and Blue indicates density gain.

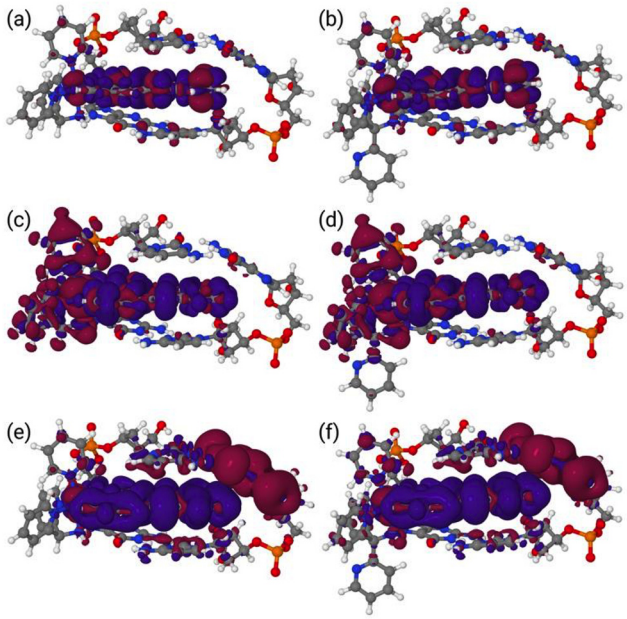

Fig. 13 Transition densities from the S_0 state in the S_0 geometry for [Ru(dipyma)(dppz)(py)]$^{2+}$ (left hand column) and [Ru(tpyma)(dppz)(py)]$^{2+}$ (right hand column) in water. Panels (a) & (b): S_0 to T_1. Panels (c) & (d): S_0 to T_2. Panels (e) & (f): S_0 to T_3. In all cases, an singlet closed-shell reference wave function was used. Red indicates density loss and Blue indicates density gain. In all cases, the bottom base pair is G–C, whereas the top pair is C–G.

marked influence on the character of the excited states of both complexes. In particular, the T_2 state now has a large ligand-ligand excitation component, whereas the T_3 state can be described as a G-dppz transition. Hereby, it should be noted that the energies of T_1–T_3 are within 0.2 eV with the next two states within an additional 0.1 eV. This means that small changes in the external environment will easily lead to changes in the ordering in the states. However, this effect should be the same for both complexes. Hence, our calculations suggest that the difference in the luminescence binding response of these two complexes is not due to a relative switching of the character of the states involved. As it is not the nature of electronic excited state of the two complexes that influences their emission response, the effect must be due to how they interact with their environment – *vide infra*.

Conclusions

This study has found that the tpyma ligand displays a somewhat unexpected (2py, NH_2) coordination motif with Ru^{II}. Given this fact, our study was extended to include the dipyma ligand which displays the same coordination pattern. A comparison between [Ru(dipyma)(dppz)(py)]$^{2+}$ and [Ru(tpyma)(dppz)(py)]$^{2+}$ revealed that -although both complexes displayed similar optical properties in water and MeCN, and almost identical binding parameters- the DNA induced luminescence enhancement for [Ru(dipyma)(dppz)(py)]$^{2+}$ is much lower than that observed for [Ru(tpyma)(dppz)(py)]$^{2+}$.

In this context, our computational studies indicated that the biggest difference between the two complexes is in the distribution of their electrostatic potentials. As the metal centre of [Ru(dipyma)(dppz)(py)]$^{2+}$ is more polar than that of [Ru(tpyma)(dppz)(py)]$^{2+}$, it is tempting to conclude that its increased electrostatic interaction with DNA and the subsequent increased perturbation of the electronic states in the triplet state leads to the observed difference in binding-induced emission. However, this would lead to an increase in the K_b for [Ru(dipyma)(dppz)(py)]$^{2+}$ compared to [Ru(tpyma)(dppz)(py)]$^{2+}$, when in fact – within experimental error – it is identical.

On the other hand, as demonstrated in Fig. 7, even in [Ru(tpyma)(dppz)(py)]$^{2+}$, the amine of the tpyma ligand can interact with surrounding solvent molecules. So, it seems likely that, when bound to duplex DNA, the less sterically hindered, more polar [Ru(dipyma)(dppz)(py)]$^{2+}$ will display greater *solvent* interactions than [Ru(tpyma)(dppz)(py)]$^{2+}$. As the light-switch effect is dependent on the isolation of the Ru^{II}(dppz) unit from water molecules, the increased solvent shielding of tpyma and the lower polarity of the Ru(tpyma)unit is likely the cause of the observed differences in the two complexes' DNA-bound emission.

Finally, it should be noted that for both complexes, DNA binding of their Ru^{II}dppz unit does not appear to be impeded as they display DNA binding affinities that are comparable to [Ru(bpy)$_2$(dppz)]$^{2+}$. As both complexes contain functional groups on the coordinated dipyma and tpyma ligands that can be used as anchor points to tether together intercalative units, they offer potential as new building blocks in the construction of structurally complex oligomeric M(dppz) systems.

Conflicts of interest

There are no conflicts to declare.

Data availability

Supporting data (synthesis details, spectroscopic and DNA binding data for [Ru(dipyma)(dppz)(py)]$^{2+}$, X-ray crystallography details, details of computational methods and calculations) have been included as part of the SI. Supplementary information is available. See DOI: **https://doi.org/10.1039/d5dt01159k**.

CCDC 2451769 and 2451848 [Ru(tpyma)(dppz)(py)]$^{2+}$ and Ru(dipyma)(dppz)(py)]$^{2+}$ contain the supplementary crystallographic data for this paper.[72a,b]

Acknowledgements

A license for the OpenEye tools,[71] obtained *via* the free Academic Licensing Program, is gratefully acknowledged. TA is grateful for the award of a studentship through EPRC CDT grant, EP/J500124/1.

References

1 A. E. Friedman, J. K. Barton, J. C. Chambron, J. P. Sauvage, N. J. Turro and J. K. Barton, *J. Am. Chem. Soc.*, 1990, **112**, 4960–4962.
2 A. W. McKinley, P. Lincoln and E. M. Tuite, *Coord. Chem. Rev.*, 2011, **255**, 2676–2692.
3 G. Li, L. Sun, L. Ji and H. Chao, *Dalton Trans.*, 2016, **45**, 13261–13276.
4 M. L. Di Pietro, G. La Ganga, F. Nastasi and F. Puntoriero, *Appl. Sci.*, 2021, **11**, 3038.
5 E. J. C. Olson, D. Hu, A. Hörmann, A. M. Jonkman, M. R. Arkin, E. D. A. Stemp, J. K. Barton and P. F. Barbara, *J. Am. Chem. Soc.*, 1997, **119**, 11458–11467.
6 B. Önfelt, P. Lincoln, B. Nordén, J. S. Baskin and A. H. Zewail, *Proc. Natl. Acad. Sci. U. S. A.*, 2000, **97**, 5708–5713.
7 J. Olofsson, B. Önfelt and P. Lincoln, *J. Phys. Chem. A*, 2004, **108**, 4391–4398.
8 M. K. Brennaman, T. J. Meyer and J. M. Papanikolas, *J. Phys. Chem. A*, 2004, **108**, 9938–9944.
9 M. Atsumi, L. González and C. Daniel, *J. Photochem. Photobiol., A*, 2007, **190**, 310–320.
10 F. E. Poynton, J. P. Hall, P. M. Keane, C. Schwarz, I. V. Sazanovich, M. Towrie, T. Gunnlaugsson, C. J. Cardin, D. J. Cardin, S. J. Quinn, C. Long and J. M. Kelly, *Chem. Sci.*, 2016, **7**, 3075–3084.
11 A. A. Cullen, C. Long and M. T. Pryce, *J. Photochem. Photobiol., A*, 2021, **410**, 113169.
12 H. Niyazi, J. P. Hall, K. O'Sullivan, G. Winter, T. Sorensen, J. M. Kelly and C. J. Cardin, *Nat. Chem.*, 2012, **4**, 621–628.
13 J. P. Hall, D. Cook, S. R. Morte, P. McIntyre, K. Buchner, H. Beer, D. J. Cardin, J. A. Brazier, G. Winter, J. M. Kelly and C. J. Cardin, *J. Am. Chem. Soc.*, 2013, **135**, 12652–12659.
14 M. R. Gill and J. A. Thomas, *Chem. Soc. Rev.*, 2012, **41**, 3179–3192.
15 A. C. Komor and J. K. Barton, *Chem. Commun.*, 2013, **49**, 3617–3630.
16 F. E. Poynton, S. A. Bright, S. Blasco, D. C. Williams, J. M. Kelly and T. Gunnlaugsson, *Chem. Soc. Rev.*, 2017, **46**, 7706–7756.
17 V. Brabec and J. Kasparkova, *Coord. Chem. Rev.*, 2018, **376**, 75–94.
18 L. Andrezálová and Z. Országhová, *J. Inorg. Biochem.*, 2021, **225**, 111624.
19 X. Li, A. K. Gorle, M. K. Sundaraneedi, F. R. Keene and J. G. Collins, *Coord. Chem. Rev.*, 2018, **375**, 134–147.
20 B. Önfelt, P. Lincoln and B. Nordén, *J. Am. Chem. Soc.*, 1999, **121**, 10846–10847.
21 L. M. Wilhelmsson, F. Westerlund, P. Lincoln and B. Nordén, *J. Am. Chem. Soc.*, 2002, **124**, 12092–12093.
22 B. Önfelt, P. Lincoln and B. Nordén, *J. Am. Chem. Soc.*, 2001, **123**, 3630–3637.
23 A. A. Almaqwashi, T. Paramanathan, P. Lincoln, I. Rouzina, F. Westerlund and M. C. Williams, *Nucleic Acids Res.*, 2014, **42**, 11634–11641.
24 A. Notaro and G. Gasser, *Chem. Soc. Rev.*, 2017, **46**, 7317–7337.
25 L. Zeng, P. Gupta, Y. Chen, E. Wang, L. Ji, H. Chao and Z. S. Chen, *Chem. Soc. Rev.*, 2017, **46**, 5771–5804.
26 K. Qiu, Y. Chen, T. W. Rees, L. Ji and H. Chao, *Coord. Chem. Rev.*, 2019, **378**, 66–86.
27 H. K. Saeed, S. Sreedharan and J. A. Thomas, *Chem. Commun.*, 2020, **56**, 1464–1480.
28 S. Monro, K. L. Colón, H. Yin, J. Roque, P. Konda, S. Gujar, R. P. Thummel, L. Lilge, C. G. Cameron and S. A. McFarland, *Chem. Rev.*, 2019, **119**, 797–828.
29 S. A. McFarland, A. Mandel, R. Dumoulin-White and G. Gasser, *Curr. Opin. Chem. Biol.*, 2020, **56**, 23–27.
30 M. Huynh, R. Vinck, B. Gibert and G. Gasser, *Adv. Mater.*, 2024, **36**, 2311437.
31 C. Metcalfe, H. Adams, I. Haq and J. A. Thomas, *Chem. Commun.*, 2003, **3**, 1152–1153.
32 S. P. Foxon, C. Metcalfe, H. Adams, M. Webb and J. A. Thomas, *Inorg. Chem.*, 2007, **46**, 409–416.
33 S. P. Foxon, M. A. H. Alamiry, M. G. Walker, A. J. H. M. Meijer, I. V. Sazanovich, J. A. Weinstein and J. A. Thomas, *J. Phys. Chem. A*, 2009, **113**, 12754–12762.
34 C. Metcalfe, I. Haq and J. A. Thomas, *Inorg. Chem.*, 2004, **43**, 317–323.
35 C. Metcalfe, M. Webb and J. A. Thomas, *Chem. Commun.*, 2002, **18**, 2026–2027.
36 H. K. Saeed, I. Q. Saeed, N. J. Buurma and J. A. Thomas, *Chem. – Eur. J.*, 2017, **23**, 5467–5477.
37 H. K. Saeed, P. J. Jarman, S. Archer, S. Sreedharan, I. Q. Saeed, L. K. Mckenzie, J. A. Weinstein, N. J. Buurma, C. G. W. Smythe and J. A. Thomas, *Angew. Chem., Int. Ed.*, 2017, **56**, 12628–12633.
38 H. K. Saeed, S. Sreedharan, P. J. Jarman, S. A. Archer, S. D. Fairbanks, S. P. Foxon, A. J. Auty, D. Chekulaev, T. Keane, A. J. H. M. Meijer, J. A. Weinstein, C. G. W. Smythe, J. Bernardino De La Serna and J. A. Thomas, *J. Am. Chem. Soc.*, 2020, **142**, 1101–1111.
39 S. P. Foxon, T. Phillips, M. R. Gill, M. Towrie, A. W. Parker, M. Webb and J. A. Thomas, *Angew. Chem., Int. Ed.*, 2007, **46**, 3686–3688.
40 P. J. Jarman, F. Noakes, S. Fairbanks, K. Smitten, I. K. Griffiths, H. K. Saeed, J. A. Thomas and C. Smythe, *J. Am. Chem. Soc.*, 2019, **141**, 2925–2937.
41 P. Arnold, S. C. Davies, J. R. Dilworth, M. C. Durrant, D. V. Griffiths, D. L. Hughes and R. L. Richards, *Inorg. Chem. Commun.*, 1998, **1**, 43–45.
42 E. Baranoff, J.-P. Collin, L. Flamigni and J.-P. Sauvage, *Chem. Soc. Rev.*, 2004, **33**, 147–155.
43 F. Richard Keene, P. J. Stephenson, M. R. Snow and E. R. T. Tiekink, *Inorg. Chem.*, 1988, **27**, 2040–2045.
44 P. J. Arnold, S. C. Davies, J. R. Dilworth, M. C. Durrant, D. V. Griffiths, D. L. Hughes, R. L. Richards and P. C. Sharpe, *J. Chem. Soc., Dalton Trans.*, 2001, **5**, 567–573.
45 M. Rezayi, R. Karazhian, Y. Abdollahi, L. Narimani, S. B. T. Sany, S. Ahmadzadeh and Y. Alias, *Sci. Rep.*, 2014, **4**, 4664.

46 A. Llobet, P. Doppelt and T. J. Meyer, *Inorg. Chem.*, 1988, **27**, 514–520.
47 C. S. Burke and T. E. Keyes, *RSC Adv.*, 2016, **6**, 40869–40877.
48 J. Chang, S. Plummer, E. S. F. Berman, D. Striplin and D. Blauch, *Inorg. Chem.*, 2004, **43**, 1735–1742.
49 E. Amouyal, A. Homsi, J. C. Chambron and J. P. Sauvage, *J. Chem. Soc., Dalton Trans.*, 1990, 1841–1845.
50 M. J. Frisch, G. W. Trucks, H. B. Schlegel, G. E. Scuseria, M. A. Robb, J. R. Cheeseman, G. Scalmani, V. Barone, G. A. Petersson, H. Nakatsuji, X. Li, M. Caricato, A. V. Marenich, J. Bloino, B. G. Janesko, R. Gomperts, B. Mennucci, H. P. Hratchian, J. V. Ortiz, A. F. Izmaylov, J. L. Sonnenberg, D. Williams-Young, F. Ding, F. Lipparini, F. Egidi, J. Goings, B. Peng, A. Petrone, T. Henderson, D. Ranasinghe, V. G. Zakrzewski, J. Gao, N. Rega, G. Zheng, W. Liang, M. Hada, M. Ehara, K. Toyota, R. Fukuda, J. Hasegawa, M. Ishida, T. Nakajima, Y. Honda, O. Kitao, H. Nakai, T. Vreven, K. Throssell, J. A. Montgomery Jr., J. E. Peralta, F. Ogliaro, M. J. Bearpark, J. J. Heyd, E. N. Brothers, K. N. Kudin, V. N. Staroverov, T. A. Keith, R. Kobayashi, J. Normand, K. Raghavachari, A. P. Rendell, J. C. Burant, S. S. Iyengar, J. Tomasi, M. Cossi, J. M. Millam, M. Klene, C. Adamo, R. Cammi, J. W. Ochterski, R. L. Martin, K. Morokuma, O. Farkas, J. B. Foresman and D. J. Fox, Gaussian 16, Revis. C.01, Wallingford CT, 2016.
51 A. D. Becke, *J. Chem. Phys.*, 1993, **98**, 5648–5652.
52 S. Grimme, S. Ehrlich and L. Goerigk, *J. Comput. Chem.*, 2011, **32**, 1456–1465.
53 M. Dolg, U. Wedig, H. Stoll and H. Preuss, *J. Chem. Phys.*, 1987, **86**, 866–872.
54 D. Andrae, U. Häußermann, M. Dolg, H. Stoll and H. Preuß, *Theor. Chim. Acta*, 1990, **77**, 123–141.
55 R. Krishnan, J. S. Binkley, R. Seeger and J. A. Pople, *J. Chem. Phys.*, 1980, **72**, 650–654.
56 A. D. McLean and G. S. Chandler, *J. Chem. Phys.*, 1980, **72**, 5639–5648.
57 F. Dröge, F. F. Noakes, S. A. Archer, S. Sreedharan, A. Raza, C. C. Robertson, S. MacNeil, J. W. Haycock, H. Carson, A. J. H. M. Meijer, C. G. W. Smythe, J. Bernardino De La Serna, B. Dietzek-Ivanšić and J. A. Thomas, *J. Am. Chem. Soc.*, 2021, **143**, 20442–20453.
58 M. Cossi, N. Rega, G. Scalmani and V. Barone, *J. Comput. Chem.*, 2003, **24**, 669–681.
59 J. Tomasi, B. Mennucci and R. Cammi, *Chem. Rev.*, 2005, **105**, 2999–3094.
60 J. D. J. D. McGhee and P. H. P. H. von Hippel, *J. Mol. Biol.*, 1974, **86**, 469–489.
61 G. Cohen and H. Eisenberg, *Biopolymers*, 1969, **8**, 45–55.
62 S. Satyanarayana, J. C. Dabrowiak and J. B. Chaires, *Biochemistry*, 1992, **31**, 9319–9324.
63 A. Kellett, Z. Molphy, C. Slator, V. McKee and N. P. Farrell, *Chem. Soc. Rev.*, 2019, **48**, 971–988.
64 I. Ortmans, C. Moucheron and A. Kirsch-De Mesmaeker, *Coord. Chem. Rev.*, 1998, **168**, 233–271.
65 I. Ortmans, B. Elias, J. M. Kelly, C. Moucheron and A. Kirsch-DeMesmaeker, *J. Chem. Soc., Dalton Trans.*, 2004, **4**, 668–676.
66 S. A. Archer, A. Raza, F. Dröge, C. Robertson, A. J. Auty, D. Chekulaev, J. A. Weinstein, T. Keane, A. J. H. M. Meijer, J. W. Haycock, S. Macneil and J. A. Thomas, *Chem. Sci.*, 2019, **10**, 3502–3513.
67 P. M. Keane, J. Tory, M. Towrie, I. V. Sazanovich, C. J. Cardin, S. J. Quinn, F. Hartl, J. M. Kelly and C. Long, *Inorg. Chem.*, 2019, **58**, 663–671.
68 M. K. Brennaman, J. H. Alstrum-Acevedo, C. N. Fleming, P. Jang, T. J. Meyer and J. M. Papanikolas, *J. Am. Chem. Soc.*, 2002, **124**, 15094–15098.
69 C. Bannwarth, S. Ehlert and S. Grimme, *J. Chem. Theory Comput.*, 2019, **15**, 1652–1671.
70 ROCS 3.7.0.1. OpenEye, Cadence Molecular Sciences, Santa Fe, NM. **https://www.eyesopen.com**; P. C. D. Hawkins, A. G. Skillman and A. Nicholls, *J. Med. Chem.*, 2007, **50**, 74–82.
71 *OEChem TK, Version 4.1.1.1*, OpenEye Scientific Software, Inc., Website: **https://www.eyesopen.com**. (Accessed 25 April 2025).
72 (*a*) T. Andrews, C. Robertson, A. J. H. M. Meijer and J. A. Thomas, CCDC 2451769: Experimental Crystal Structure Determination, 2025, DOI: **10.5517/ccdc.csd.cc2n98bl**; (*b*) T. Andrews, C. Robertson, A. J. H. M. Meijer and J. A. Thomas, CCDC 2451848: Experimental Crystal Structure Determination, 2025, DOI: **10.5517/ccdc.csd.cc2n9bw6**.